JOURNAL OF MATERIALS SCIENCE 37 (2002) 4437–4443

Residual stresses in particle-reinforced ceramic composites using synchrotron radiation

MYUNGAE LEE, YANAN XIAO, D. E. WITTMER
Department of Mechanical Engineering and Energy Processes, Southern Illinois University at Carbondale, Carbondale, IL 62901, USA
E-mail: lee@cars.uchicago.edu

T. J. GRABER
The Center for Advanced Radiation Sources, The University of Chicago, Chicago, IL 60637, USA

S. M. MINI
Department of Physics, Northern Illinois University, De Kalb, IL 60115, USA; Material Science Division, Argonne National Laboratory, Argonne, IL 60439, USA

Residual stresses were determined in particle-reinforced ceramic composites using synchrotron based x-ray diffraction. The baseline Si_3N_4 and the Si_3N_4-TiN composites were processed by turbomilling, pressure casting, and isopressing. They were then continuously sintered to full density, under a pressureless, flowing nitrogen atmosphere. The flexural strength, fracture toughness, and residual stress were measured for as-machined samples and following quenching in water from 1000°C, 1100°C, and 1200°C. The residual stresses for both the baseline Si_3N_4 and the Si_3N_4-TiN composites were determined from the (441) and (531) reflections, by applying the 2θ-$\sin^2\psi$ method. The measured residual stresses were compared with the flexural strength and fracture toughness results to determine the effects of residual stress and thermal shocking on the mechanical properties of each material. In both the baseline Si_3N_4 and Si_3N_4-TiN composites, after thermal shocking, the compressive residual stresses were developed in directions both parallel and perpendicular to the sample surface. The residual compressive stresses for the Si_3N_4-TiN composites were much higher than the baseline Si_3N_4. As a result, both fracture toughness and flexural strength of the Si_3N_4-TiN composites were improved. In addition, the addition of the TiN appears to improve both the strength and toughness of the baseline Si_3N_4.

1. Introduction

Advanced structural ceramics have gained increasing interest as promising materials in diverse fields of modern engineering. Of these advanced ceramics, silicon nitride (Si_3N_4) has maintained the strong interest of researchers as an alternative material to be used in the advanced heat engines and other applications requiring high strength, excellent wear resistance, lower thermal expansion, and oxidation resistance at elevated temperature. The need to further improve mechanical reliability, which is the combination of high strength and fracture toughness, of Si_3N_4 has been addressed by adding particulates, whiskers, or continuous fibers to the monolithic Si_3N_4 [1, 2]. Although toughening of particulate composites is not so high in comparison with that of other composites, particles have been mostly used as reinforcements for SiC and Si_3N_4, due to easier processing and lower cost than whiskers and fibers [3].

However, since ceramic materials are brittle and have a high surface sensitivity, it is very important to control the fracture behavior in order to design high quality materials. Some damage on the surface of this brittle material, caused by fabrication processing and machining, are in the form of residual stresses and cracks in and just below the surface. Even in the ceramic matrix composites, toughened by the addition of the second phase into ceramic matrix to get better mechanical properties and reliability, residual stress exists due to the thermal expansion mismatch between matrix and reinforcement [4]. These residual stresses can lead to crack initiation in the sense of microcracking, influence crack propagation, and contribute to the effectiveness of crack bridging [5]. Therefore, understanding the role of interfacial and bulk residual stress on strength, toughness, and fatigue may improve processing and hence the physical and mechanical properties of ceramics and ceramic matrix composites.

X-ray diffraction techniques have been used extensively to determine the residual stress in ceramics and ceramic matrix composites. Such measurements have been performed using Cr K_α and Cu K_α radiation on the ground surface layer of Si_3N_4 [6, 7], Al_2O_3 [8],

and SiC [9]. Several investigations of residual stress in Al_2O_3/SiC whisker composite system have also been reported [10–12]. Predecki *et al*. [13] studied a hot pressed α-Al_2O_3 composite containing 25 wt% β-SiC whiskers. They suggested that due to the texture, which developed more in the whisker than in the matrix, the matrix could relax to a greater extent in the hot pressing direction than in the transverse direction; resulting in decreasing the residual stress in the hot pressing direction. Magley *et al*. [14] investigated the residual stress in SiC/TiB_2 particle composite. They measured the residual stress before and after bending the samples to fracture. Tensile residual stress in TiB_2 and compressive residual stress in SiC as the microstress decreased by nearly 60% after bending. It was believed that this system undergoes microcracking as a toughening mechanism. The triaxial state of the loading and thermal residual stresses in ZrO_2/Al_2O_3 was measured by Tanaka *et al*. [15]. The residual stress in Al_2O_3 phase was compression and decreased linearly with Al_2O_3 volume fraction, while that in the ZrO_2 phase was tension and increased linearly with Al_2O_3 volume fraction.

However, many diffraction profiles in ceramics, by applying radiation from different conventional x-ray tubes, appear either with over-lapping between neighboring planes or with small intervals between diffracting planes, due to their complex crystal structures [16]. In addition, the diffraction spectra for the ceramic matrix composites show the super-positions of the diffraction profiles, due to the different crystalline phases. Recently, the application of synchrotron radiation diffraction for stress analysis opens the possibility to investigate ceramics and ceramic matrix composites, because it offers a high-radiation flux and the choice of tunable sources of monochromatic, pink, and white radiation [9, 17].

The purpose of this study is to determine the residual stresses in silicon nitride based materials that have been subjected to thermal shock treatment and to demonstrate the utilization of a high-energy synchrotron radiation for diffraction studies.

2. Experimental procedure

2.1. Materials

A Si_3N_4 baseline composition, containing 3 wt% Al_2O_3 (Grade HPA-0.5 AF, Ceralox, Corp., Tuscon, AZ) and 9 wt% Y_2O_3 (Grade HP, H. C. Strack, Inc., NY, NY), and Si_3N_4-Tin composities, also containing 5 wt% TiN (Grade C, H. C. Starck, Inc., NY, NY) as a particulate addition, were investigated. The overall raw materials were turbomilled with 3-mm-diameter silicon nitride media for 2 h at 1200 rpm. The resulting slurry was sieved through a 20/325-mesh screen stack. After deairing for 1 h, the slurry was pressure cast into green disks 7.6 cm in diameter by approximately 2.2 cm thick, using a commercial filter press (API Filter Press, Baroid Testing Equipment, Houston, TX) and then dried under vacuum for 24 h. Following drying, the disks were cold iso-statically pressed at 350 MPa. The green compacts were then sintered in a Model 44-BF continuous belt furnace (Centorr Vacuum Industries, Nashua, NH) at 1775°C for 2 h under a pressureless nitrogen atmosphere.

The sintered disks were machined into rectangular bars in dimensions of 3 mm × 4 mm × 45 mm for measurement of mechanical properties and residual stresses. Test bars from each composition were then subjected to thermal shocking at 1000°C, 1100°C, and 1200°C. Thermal shocking was accomplished by heating the test bars in a flowing nitrogen atmosphere to the desired thermal shocking temperature for 30 min, followed by room temperature water quenching. The test bars rested on boron nitride (BN) boats while being gradually heated to the specified temperature. The boats were removed from the furnace, and the bars were immediately dropped into the water baths. Utilization of the boats was to prevent spot quenching on the hot bars by any tool that would have been used to remove them from the furnace.

Flexural strength was measured by a four-point bending test on an Universal Testing Machine (Model 1101, Applied Test Systems Inc., Butler, PA). As-machined and thermally shocked samples were fractured at a cross-head speed of 0.5 mm/min at room temperature, with the inner and outer spans of 20 mm and 40 mm, respectively. Fracture toughness (K_{IC}) was determined by a modified indentation technique with a 5-kg load using Vickers indentation [18]. The tensile surfaces for fracture toughness measurements were diamond polished to a 0.5-μm finish, prior to fracture.

2.2. Strain measurements

X-ray measurements were made using conventionally generated x-rays and synchrotron radiation. First of all, x-ray diffraction experiment was performed using rotating anode Cu tube x-ray source (Rigaku-Geigerflex, Rigaku USA, Danvers, MA). The x-ray generator parameters were set at 40 kV and 140 mA. Scan speed was 0.4/min. The measurement were accomplished in $\theta/2\theta$ mode with an accounting time of 3 sec at each data point. The diffractometer contained a position sensitive proportional counter and focusing crystal, which was a curved graphite monochromator. This curved monochromator served as directional filter to eliminate unwanted fluorescence and other scattered characteristic radiation. Thus, Cu K_β radiation was filtered by means of this monochromator.

Synchrotron x-ray diffraction in the angle dispersive x-ray diffraction (ADXD) configuration was carried out at the 12-BM-D beamline of the Basic Energy Sciences Synchrotron Radiation Center (BESSRC) at the Advanced Photon Source (APS). The x-ray beam produced by a bending magnetic was monochromated and tuned to the energy of 8.856 keV (corresponding to a wavelength of $\lambda \approx 1.4$ Å), using a water-cooled double Si (111) crystal and focused in the horizontal direction at the sample position by a Rh-coated Si mirror. The diffracted beam was collected using a scintillation counter with a Ge (111) crystal analyzer, installed on the 2θ arm. This analytic crystal would provide excellent angular resolution and a good signal-to-noise ratio. The samples were mounted on the flat-plate holder and

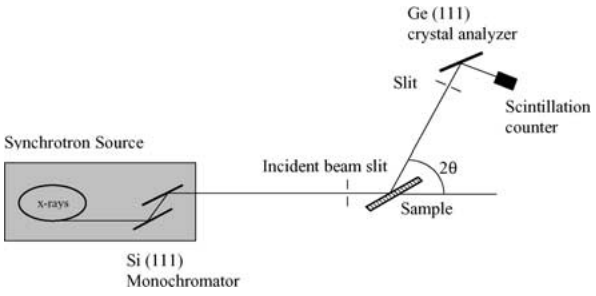

Figure 1 Configuration for synchrotron x-ray diffraction (BESSRC, APS).

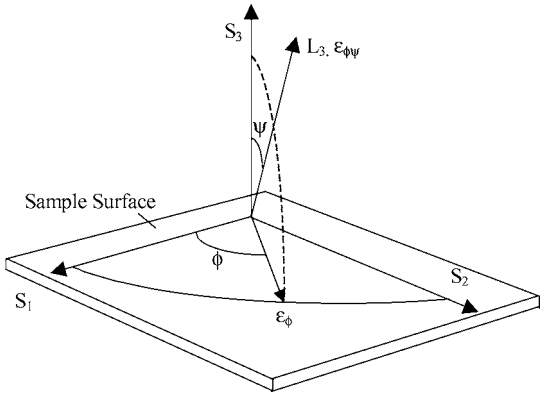

Figure 2 Definition of coordinate systems and angles.

tilted with respect to the theta axis. The schematic of the experimental set-up is shown in Fig. 1.

The 4-circle Huber diffractometer (Blake Industries Inc., Scotch Plains, NJ) was step-scanned over the 2θ range 101° to 105° at a 0.01° 2θ-step interval and with step times of 3 to 7 sec. This was sufficient to keep the photon count consistent. The tilting angles (ψ) were selected to be 0°, ±16.43°, ±23.58°, ±29.33°, and ±34.45° for an even distribution of $\sin^2\psi$ values.

In order to obtain the stress-free interplanar spacing, the strain measurements were made on powdered samples of both the baseline Si_3N_4 and the Si_3N_4-TiN composite under the same conditions. These powdered samples were prepared by crushing and grinding one of the test bars from each composition in a vibratory/shaker mixer (SPEX Mixer), which used a tungsten carbide liner and tungsten carbide impacter. The powders were then deposited on a plastic wafer substrate for analysis.

2.3. Stress analysis

The diffraction method is based on the determination of residual stress state on the surface of sample by measuring the inter-planar spacing at each sample orientation, as defined by the two angles, ϕ and ψ, shown in Fig. 2 [19]. In the conventional x-ray stress analysis, a biaxial stress state, which is uniform in the surface layers penetrated by the x-ray beam, may be assumed because this penetration depth is too shallow to be affected by the stresses in the direction of the surface normal [20]. As a result, all stress components σ_{3i} ($i = 1, 2, 3$) will vanish at the surface of the specimen. However, this biaxial stress analysis has been shown to be unsuitable for most cases and hence has led to inconsistent results in the calculation of the stress on the surface of a material [21, 22].

If the penetration depth of the x-ray is larger or at least comparable to the grain size and if the material is polyphase, as in the Si_3N_4 and the Si_3N_4-TiN composites, finite values of σ_{33} do exist, along with the stresses in the direction parallel to the surface (σ_{11}). Therefore, the stress analysis should be extended to the triaxial case, including σ_{33} in the stress calculation:

$$\varepsilon_{\phi\psi} = \frac{1+\nu}{E}\left(\sigma_{11}\cos^2\phi + \sigma_{12}\sin 2\phi + \sigma_{22}\sin^2\phi - \sigma_{33}\right)\sin^2\psi + \frac{1+\nu}{E}\sigma_{33} - \frac{\nu}{E}(\sigma_{11}+\sigma_{22}+\sigma_{33}) + \frac{1+\nu}{E}(\sigma_{13}\cos\phi + \sigma_{23}\sin\phi)\sin 2\psi \quad (1)$$

With differentiating Bragg's law and definition of strain, the stresses can be determined as follows:

$$2\theta = 2\theta_0 - 2\tan\theta_0\left(\frac{1+\nu}{E}\right)(\sigma_{11}-\sigma_{33})\sin^2\psi + 2\tan\theta_0\frac{\nu}{E}\left(2\sigma_{11} - \frac{\sigma_{33}}{\nu}\right) \quad (2)$$

where ν, E, and θ_0 are Poisson's ratio, Young's modulus, and the Bragg's angle of the unstressed material, respectively. Here it is assumed that no shear stress components exist and $\sigma_{11} = \sigma_{22}$.

3. Results and discussion

3.1. Residual stress in the baseline Si_3N_4

The diffraction pattern of the as-machined Si_3N_4 sample using the rotating anode source is shown in Fig. 3. The α_1 and α_2 doublet from Cu K_α radiation, which is one of the largest problems with the rotating anode source, was observed for each diffraction peak. As can be seen, the diffraction peaks at higher angle were well resolved. It has been known that the strongly diffracted peaks at a high 2θ are desired because those peaks will

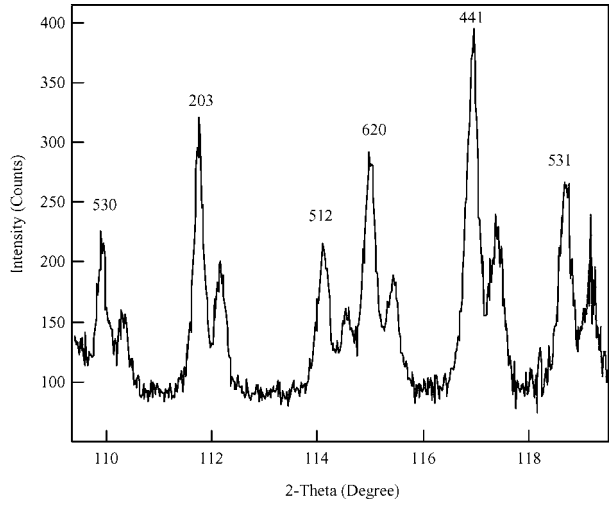

Figure 3 Diffraction pattern of the as-machined Si_3N_4 sample, using conventional rotating anode x-ray source.

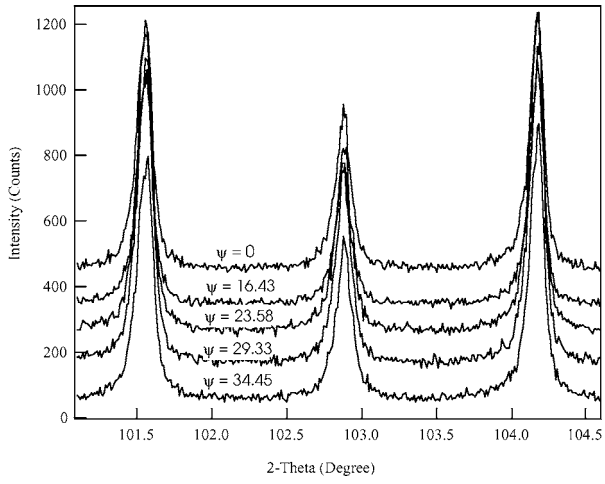

Figure 4 High-angle diffraction patterns obtained from the synchrotron radiation for the as-machined Si_3N_4 sample at different tilted angles.

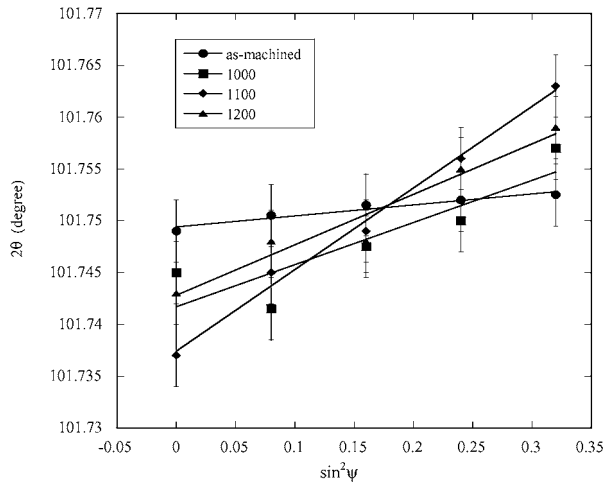

Figure 5 Relationship between the centroid peak positions, corresponding to the baseline Si_3N_4 (441) plane, and different tiltied angles.

display a larger shift in 2θ as well as provide consistency and reliability in determining the angular position of the peaks. Therefore, the high angle diffraction peaks corresponding to (441) and (531) planes were chosen to be used in the residual stress analysis.

Although those selected peaks from (441) and (531) planes were well resolved, the centroid peak position could not be determined with high precision, due to the low signal-to-noise ratio. The accuracy of x-ray diffraction residual stress measurement depends on the precision with which the diffraction peak can be located. According to Sahiner *et al*. [7], when the residual stresses in the Si_3N_4 sample were determined using the conventional x-ray source, the deviations of the angular peak positions from the x-ray diffraction data were substantially high in the 2θ vs. $\sin^2\psi$ diagram. This was a result of not being able to resolve the angular position of the peaks with high precision. Since the imprecise peak positions prevented the linear fit from being conclusive, the residual stress results of the Si_3N_4 sample were not consistently produced.

Besides the $K_{\alpha 1}$ and $K_{\alpha 2}$ doublets problem, the diffraction patterns obtained from with a standard Bragg–Brentano diffractometer showed the peak broadening as the sample was titled. It could be because the sample parafocused the beam back on the exit slit. Due to the low resolution of the radiation from the conventional rotating anode source and the lack of accuracy of the diffractometer alignment, synchrotron x-ray was used for this study.

The high angle diffraction patterns of the as-machined sample using synchrotron x-ray as a function of 2θ angles are given in Fig. 4. As was expected, the peaks were of relatively high intensity and fairly symmetric. The peaks also had the narrow widths, which would be an advantage for the determination of the peak position. In order to determine the peak position accurately, which is necessary for the residual stress analysis, a profile analysis was performed on all of the collected raw data, using an in-house fitting program. This fitting program included background subtraction, smoothing, and centroid determination. The background was subtracted by a linear fit to the data and each peak was smoothed using a Fourier and Inverse Fourier Transformation.

Once the locations of each peak were found, the 2θ-$\sin^2\psi$ method was employed to determine the residual stresses in the bulk of the Si_3N_4. The in-plane shear stresses were considered to be negligible when ϕ was varied from 0° to 90° (i.e., $\sigma_{11} = \sigma_{22}$). Furthermore, it was assumed that the average of out-of-plane shear stresses, σ_{13} and σ_{23}, could be neglected. Thus, only two unknown stresses, σ_{11} and σ_{33}, should be determined. Fig. 5 shows the diffraction peak positions for the (441) reflection from the baseline Si_3N_4 samples as a function of $\sin^2\psi$. The slopes obtained from the thermally shocked samples appeared to be steeper than the as-machined sample, indicating the development of compressive residual stresses, due to thermal treatment. The thermally shocked sample from 1100°C exhibited the largest slope, which resulted in the highest compressive residual stress. The deviations from the linear curve fit were less than 0.001° for all data points, except the points of the sample thermally shocked from 1000°C, which was about 0.004°. The diffraction data for the (531) reflection exhibited similar behavior.

By using the diffraction angle, $2\theta_0$, measured from the powdered sample, and the values of the slope and intercept obtained from Fig. 5, the residual stresses in the directions parallel (σ_{11}) and perpendicular (σ_{33}) to the surface were calculated according to Equation 2. The elastic constants used for these calculations were Poisson's ratio (ν) = 0.27 and Young's modulus (E) = 304 GPa [7]. The average values of σ_{11} and σ_{33}, obtained from both (441) and (531) planes, and the results of flexural strength and fracture toughness at different thermal shocking temperatures are summarized in Table I. The average values of flexural strength and fracture toughness were obtained based on 5 times measurements. When a comparison was made between the as-machined and the thermally shocked samples, a significant increase in both σ_{11} and σ_{33} was observed. The residual stresses for the baseline Si_3N_4, induced by thermal shocking, were found to be in compression for both directions. The residual stresses in the direction parallel to the surface were much higher than in the

TABLE I Average values of residual stresses, fracture toughness, and flexural strength in the baseline Si_3N_4

	Residual stress (MPa)				
	Triaxial		Biaxial		
Temperature (°C)	$\langle\sigma_{11}\rangle$	$\langle\sigma_{33}\rangle$	$\langle\sigma_{11}\rangle$	Flexural strength (MPa)	Fracture toughness (MPa$\sqrt{m}$)
As-machined	−18	0	−20	920	6.6
1000	−100	−26	−80	930	7.3
1100	−190	−73	−140	670	5.5
1200	−110	−35	−86	190	2.3

perpendicular direction. These results showed a trend of increasing compressive residual stresses with increasing thermal shocking temperature. After reaching the maximum at the thermal shock temperature of 1100°C for both σ_{11} and σ_{33}, the compressive residual stresses was found to decrease in both directions. It is likely that the compressive stresses increase until cracks occurred on the samples' surfaces.

Biaxial residual stress values of the baseline Si_3N_4 showed a similar increasing trend with increasing thermal shocking temperatures. The results confirmed an increase in the compression in the surface after thermally shocking. However, the values determined have the potential errors caused by the penetration of the x-ray beam into the stress gradient. In the biaxial analysis, the assumption was made that the residual stress was constant throughout the depth of penetration of the incident x-ray beam. Unfortunately, for most materials of practical interest, the stress varies with the depth beneath the surface.

Since the presence of compressive residual stresses in the materials has been known to increase the strength and toughness, the highest strength and toughness would be expected to be in the sample thermally shocked from 1100°C [4]. It has to be considered that the depth of the cracked surface layer and the thickness of the layer affected by compressive residual stresses have competitive effects on the flexural strength. As can be seen, the measured results of strength and toughness were not completely consistent with those of residual stress. It might come from the errors from the $\sin^2\psi$ fits for each reflection. A variation of focal point, beam divergence, and sample displacement would possibly lead to instrumental errors in residual stress measurement.

3.2. Residual stress in the Si_3N_4/TiN composites

Fig. 6 shows the diffraction patterns for both the baseline Si_3N_4 and Si_3N_4-TiN samples thermally shocked from 1100°C. In the Si_3N_4-TiN composite, since the thermal expansion of the TiN particles is larger than that of the Si_3N_4 matrix, it has been determined that TiN particles are under isostatic tensile stress, while the Si_3N_4 matrix is under radial tensile and tangential compressive stresses simultaneously. As can be seen, the diffraction peaks of Si_3N_4-TiN samples shifted to a higher angle. This means that the influence on the Si_3N_4 lattice of the compressive stress was greater than that of the tensile stress. The diffraction patterns had the peaks of the main constituent phase, which was the Si_3N_4 phase. No other phase was detected.

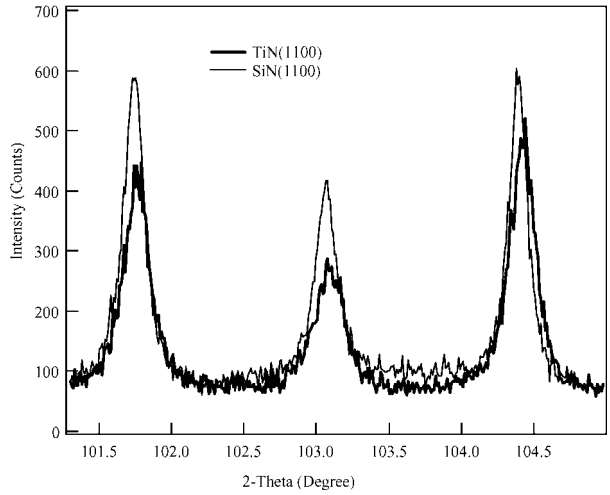

Figure 6 Diffraction patterns of the baseline Si_3N_4 and Si_3N_4-TiN samples thermally shocked at 1100°C. TiN and SiN represent the Si_3N_4-TiN composite and the baseline Si_3N_4, respectively.

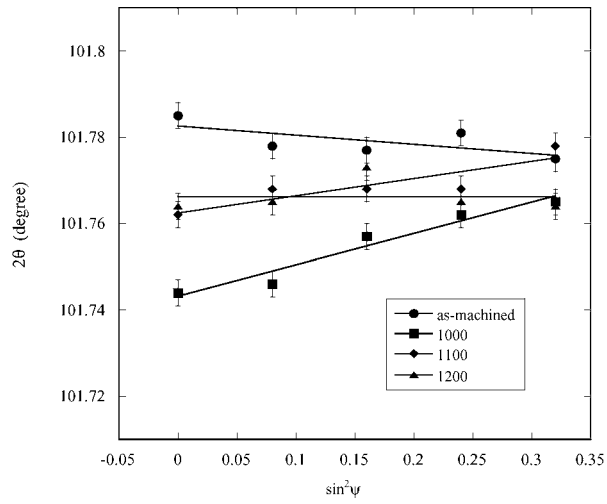

Figure 7 Relationship between the peak positions, corresponding to the Si_3N_4-TiN (441) plane, and different tilted angles.

After the centroids of the individual peaks were found, the same method was used for the 2θ-$\sin^2\psi$ calculations, as was used previously. Fig. 7 indicates the relation between 2θ and $\sin^2\psi$, corresponding to the (441) reflection, for all of the Si_3N_4-TiN composites. For all cases, the variation of 2θ with $\sin^2\psi$ could be considered to be linear, within experimental error, with no ψ splitting. With respect to the experimental error in this experiment, the system error and statistical error were 0.0012° and 0.0017°, respectively. The system error might be associated with some factors

TABLE II Average values of residual stresses, fracture toughness, and flexural strength in the Si_3N_4-TiN composites

	Residual stress (MPa)				
	Triaxial		Biaxial		
Temperature (°C)	$\langle\sigma_{11}\rangle$	$\langle\sigma_{33}\rangle$	$\langle\sigma_{11}\rangle$	Flexural strength (MPa)	Fracture toughness (MPa$\sqrt{m}$)
As-machined	−35	−59	−30	900	6.6
1000	−230	−80	−150	930	7.7
1100	−140	−74	−70	890	6.3
1200	−100	−54	−17	850	6.1

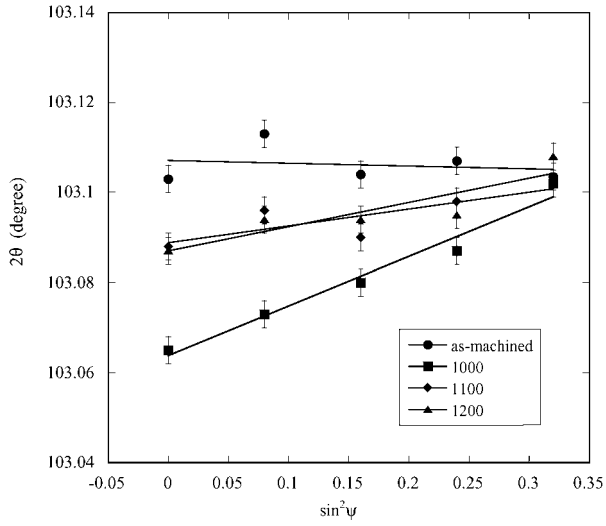

Figure 8 Relationship between the peak positions, corresponding to the Si_3N_4-TiN (531) plane, and different tilted angles.

such as reproducibility of the goniomer, detuning of the monochromator, etc.

The deviations from the least square linear curve fit were less than 0.006° for all the data points. The substantially lower deviations were a result of being able to better resolve the angular positions of the diffraction peaks from the diffraction patterns. This would be expected to aid in the accuracy of the residual stress calculations. For the as-machined sample, the slope appears to be only slightly negative, which would be evidence of the reduction of the compressive stress or some the tensile stress. Also, the slope of the thermally shocked sample from 1200°C was either very close to zero or slightly negative. However, a very steep slope was obtained for the thermally shocked sample from 1000°C. For the (531) refection, similar results were produced from all the samples, as shown in Fig. 8.

By following the same calculation procedure, used previously for the baseline Si_3N_4, both residual stresses parallel (σ_{11}) and perpendicular (σ_{33}) to the sample surface were determined. The mechanical values used for these calculations were $\nu = 0.27$ and $E = 313.22$ GPa, which was determined from the rule of mixture by taking 470 GPa for TiN and 304 GPa for Si_3N_4 [23, 24]. Table II gives the average of residual stress and the flexural strength and fracture toughness results of the Si_3N_4-TiN composites at the various thermal shocking temperatures. The results from Table II show the critical shocking temperature would be about 1000°C. This would be the temperature expected to develop the most surface compression in the Si_3N_4-TiN composites. The dependence of mechanical properties on the thermal shocking temperature for the Si_3N_4-TiN composites was consistent with the residual stress results obtained from synchrotron x-ray diffraction. The residual compressive stresses for the Si_3N_4-TiN composites were much higher than the baseline Si_3N_4.

The highest flexural strength was observed for the test bar that was thermally shocked from 1000°C. The as-machined sample with 5 wt% TiN showed the slightly lower strength compared with the baseline Si_3N_4. This might be attributed to the lack of grain growth of the reinforcing β-Si_3N_4 grains. It was observed that the β-Si_3N_4 grains, in the Si_3N_4-TiN composites, did not achieve the same aspect ratio as the baseline.

Similarly, an increase in fracture toughness was observed at 1000°C. Although the fracture toughness of the as-machined Si_3N_4-TiN composite was same as that of the baseline, an improved fracture toughness was observed, due to the addition of small quantities of TiN, at all of the higher thermal shocking temperatures. The increases in the flexural strength and the fracture toughness of Si_3N_4-TiN composites might be explained by evaluation of the residual stresses. The TiN particulates having a higher thermal expansion coefficient may have created a complicated stress field around the TiN particles because of the thermal expansion mismatch. These stresses could improve the flexural strength and the fracture toughness, due to a longer crack path with a region of compressive residual stresses around the TiN grains and microcracking in the vicinity of the TiN particles.

4. Conclusion

In this study, the effect of heat treatment on the residual stresses measured by synchrotron x-ray diffraction method for the baseline Si_3N_4 and the Si_3N_4-TiN composites are reported. The mechanical properties for these composites were found to be dependent on the compressive residual stresses, as related to the thermal shocking temperature. For both the baseline Si_3N_4 and the Si_3N_4-TiN composites, the average residual stresses in the direction parallel to the sample surface were much higher than in the perpendicular direction. The results suggested that there should be a maximum thermal shock temperature within the range of 1000°C to 1100°C for improving fracture toughness for both the baseline Si_3N_4 and the Si_3N_4-TiN composites. The high intensity of synchrotron radiation leaded to reasonable counting time for data acquisition and much better signal-to-noise ratio with respect to conventional x-ray sources. Therefore, the use of synchrotron x-ray

radiation allowed the determination of the residual stress for the particle-reinforced ceramic materials with high precision.

Acknowledgements

This research was supported by the Illinois Board of Higher Education through the HECA grant supporting the X-ray Collaboration for Illinois Technology and Education, Advanced Photon Source Project and the grant funding from the Department of Energy through Oak Ridge National Laboratory. Use of the Advanced Photon Source was supported by the U.S. Department of Energy, Office of Science, and Office of Basic Energy Sciences under Contract No. W-31-109-ENG-38. In addition, valuable help from BESSRC staffs is gratefully acknowledged.

References

1. C. J. SHIN, J. M. YANG and A. EZIS, *Scr. Metall.* **24** (1990) 2419.
2. S. T. BULJAN and V. K. SARIN, *Composites* **18** (1987) 129.
3. Y. G. GOGOTSI, *J. Mater. Sci.* **29** (1994) 2541.
4. M. TAYA, S. HAYASHI, A. S. KOBAYASHI and H. S. YOON, *J. Amer. Ceram. Soc.* **73** (1990) 1382.
5. A. G. EVANS, *Acta. Metall.* **26** (1978) 1845.
6. T. HANABUSA, H. FUJIWARA and Y. FUJIMOTO, in "International Conferences on Residual Stresses," edited by G. Beck, S. Denis and A. Simon (Elsevier Science, London, 1989) p. 310.
7. A. SAHINER, D. E. WITTMER and M. SWEENY, *Nucl. Instrum. Meth.* B **133** (1997) 73.
8. C. BURMAN and T. ERICSSON, in "International Conferences on Residual Stresses," edited by G. Beck, S. Denis and A. Simon (Elsevier Science, London, 1989) p. 368.
9. K. TANAKA, K. SUZUKI and Y. YAMAMOTO, in "International Conferences on Residual Stresses," edited by G. Beck, S. Denis and A. Simon (Elsevier Science, London, 1989) p. 15.
10. X. ZHU and P. PREDECKI, *Adv. X-ray Anal.* **39** (1996) 371.
11. M. ODEN, T. ERICSSON and J. B. COHEN, *ibid.* **39** (1996) 391.
12. A. ABUHASAN, C. BALASINGH and P. PREDECKI, *J. Amer. Ceram. Soc.* **73** (1990) 2474.
13. X. ZHU and P. PREDECKI, *Ceram. Eng. Sci. Proc.* **12** (1991) 1574.
14. D. J. MAGLEY, R. A. WINHOLTZ and K. T. FABER, *J. Amer. Ceram. Soc.* **73** (1990) 1641.
15. K. TANAKA, *Adv. X-ray Anal.* **36** (1993) 473.
16. Y. YOSHIOKA, H. MATSUI, T. MOROOKA, K. HASEGAWA and M. KOIKE, in "Residual Stresses in Science and Technology," edited by E. Macherauch and V. Hauk (Informationsgesellschaft-Verlag, Oberursel, 1987) p. 369.
17. B. EIGENMANN and E. MACHERAUCH, *Nucl. Instrum. Meth.* B **97** (1995) 92.
18. P. CHANTIKUL, G. R. ANSTIS, B. R. LAWN and D. B. MARSHALL, *J. Amer. Ceram. Soc.* **64** (1981) 539.
19. I. C. NOYAN and J. B. COHEN, "Residual Stress, Measurement by Diffraction and Interpretation" (Springer-Verlag, New York, 1987)
20. B. D. CULLITY, "Elements of X-ray Diffraction" (Addison-Wesley, Massachusetts, 1978).
21. H. RUPPERSBERG, *Adv. X-ray Anal.* **35** (1992) 481.
22. K. TANAKA, *ibid.* **36** (1993) 473.
23. Engineering Property Data on Selected Ceramics, Vol.1, Nitrides, Battelle Columbus Laboratories, MCIC-HB-07 (1976).
24. H. J. CHOI, K. S. CHO and J. G. LEE, *J. Amer. Ceram. Soc.* **80** (1997) 2681.

Received 8 October 2001
and accepted 20 June 2002